

Electric field controlled valley-polarized photocurrent switch based on the circular bulk photovoltaic effect

Yaqing Yang,^{1,5} Xiaoyu Cheng,^{1,5} Liantuan Xiao,^{1,5} Suotang Jia,^{1,5} Jun Chen,^{2,5,*} Lei Zhang,^{1,5,†} and Jian Wang^{3,4,‡}

¹State Key Laboratory of Quantum Optics and Quantum Optics Devices,
Institute of Laser Spectroscopy, Shanxi University, Taiyuan 030006 China

²State Key Laboratory of Quantum Optics and Quantum Optics Devices,
Institute of Theoretical Physics, Shanxi University, Taiyuan 030006, China

³College of Physics and Optoelectronic Engineering, Shenzhen University, Shenzhen 518060, China

⁴Department of Physics, The University of Hong Kong, Pokfulam Road, Hong Kong, China

⁵Collaborative Innovation Center of Extreme Optics, Shanxi University, Taiyuan 030006, China

Efficient electric manipulation of valley degrees of freedom is critical and challenging for the advancement of valley-based information science and technology. We put forth an electrical scheme, based on a two-band Dirac model, that can switch the fully valley-polarized photocurrent between K and K' valleys using the circular bulk electro-photovoltaic effect. This is accomplished by applying an out-of-plane electric field to the two-dimensional valley materials, which enables continuous tuning of the Berry curvature and its sign flip. We found that the switch of the fully valley-polarized photocurrent is directly tied to the sign change of Berry curvature, which accompanies a topological phase transition, for instance, the quantum spin Hall effect and the quantum valley Hall effect. This scheme has been confirmed in monolayer BiAsI₂ and germanene through first-principles calculations. Our paper offers a promising strategy for the development of a volatile valley-addressable memory device and could inspire further research in this area.

Introduction—Recently, significant research interest has emerged in the development of electronic devices that utilize factors other than an electron’s charge degrees of freedom^{1–6}. Along with spintronics^{7–10}, the valley degrees of freedom in solid materials, such as graphene^{11–13} and transition metal dichalcogenides^{14–17}, can be harnessed for information encoding, storage, and transportation^{18–20}. To use valley degrees of freedom as information carriers, it is necessary to generate and efficiently control the valley polarization^{21–24}. Electric field tuning is a low-power and efficient approach applied to certain two-dimensional valley materials to adjust valley polarization^{25–39}. However, the direct use of electric-induced valley switching as a volatile valley-addressable memory device remains unexplored.

When two-dimensional valley materials are exposed to circularly polarized light, electrons in K/K' valleys can be selectively excited depending on the light polarization. This process produces a fully valley-polarized photocurrent^{40–42}. Recently, the out-of-plane electric field has been presented to control the direction and magnitude of the charge photocurrent due to the electrically switchable Berry curvature dipole⁴². As such, it is worth exploring if the fully valley-polarized photocurrent can be electrically toggled between K and K' valleys by adjusting the quantum geometrical quantity, for instance, Berry curvature. It is our work to fill this gap.

In this paper, we propose a scheme to effectively control and switch the fully valley-polarized photocurrent through an out-of-plane electric field. Based on a two-band Dirac model, we analytically show that the fully valley-polarized photocurrent can be switched between K and K' valleys through the circular bulk electro-photovoltaic effect (CBEPV). The fundamental physical mechanism involves changing the sign of Berry curvature in two-dimensional valley materials by applying an out-of-plane electric field. It is found that this change accompanies a topological phase transition between the quan-

tum spin Hall effect (QSHE) and the quantum valley Hall effect (QVHE), or a transition between different QVHE states. The change in the sign of the Berry curvature alters both the valley-dependent optical selection rule and the CBEPV-induced valley-dependent photocurrent, which leads to the switching of the fully valley-polarized photocurrent. Based on atomic first-principles calculations, we present that the fully valley-polarized photocurrent in monolayer BiAsI₂ and germanene can be switched between K and K' valleys by tuning the out-of-plane electric field. Our paper demonstrates the significant potential of two-dimensional valley materials for use in volatile valley-addressable memory devices.

Berry curvature analysis—We start from the interband optical transition at a \mathbf{k} point in the two-band model. The degree of circular polarization $\eta_{\tau_z}(\mathbf{k})$ can be expressed as⁴³

$$\eta_{\tau_z}(\mathbf{k}) = \frac{e}{2\hbar} \frac{\Omega_{\tau_z}^v(\mathbf{k})}{\mu_B^*} E_{\mathbf{k},21} \quad (1)$$

where $\Omega_{\tau_z}^v(\mathbf{k})$ is the out-of-plane Berry curvature of the valance band. $\tau_z = \pm 1$ denotes K and K' valleys, respectively. $E_{\mathbf{k},21} = E_{\mathbf{k},2} - E_{\mathbf{k},1}$ is the energy difference between two bands at the \mathbf{k} point, 1 and 2 correspond to valence and conduction bands, and μ_B^* is the effective Bohr magneton. The $\eta_{\tau_z} = 1$ and -1 values correspond to the absorption of only left (σ_+) and right (σ_-) circularly polarized light, respectively. This suggests that if the Berry curvature’s sign for a specific valley is reversed by applying the out-of-plane electric field, while the sign of $E_{\mathbf{k},21}$ is maintained, the corresponding valley-dependent optical selection rules at K and K' can be switched, which is depicted in Fig. 1 (a).

Circularly polarized light is known to produce an injection current in materials when the time reversal symmetry is maintained while the inversion symmetry is broken. The circular photovoltaic/photogalvanic effect (CPGE) induced photocurrent is given by $dJ/dt = dJ^{\sigma_+}/dt - dJ^{\sigma_-}/dt = \beta_{bc}^a E_b(\omega) E_c(-\omega)$ ^{41,44,45}, where β_{bc}^a is the CPGE tensor and

$E_{b,c}$ is the optical electric field. For a two-band model containing the valence band and the conduction band, the valley-dependent CPGE tensor can be expressed as^{41,44}

$$\begin{aligned}\beta_{bc}^{a,\tau_z}(\omega) &= \sum_{\mathbf{k} \in \tau_z} \beta_{bc}^a(\mathbf{k}) \\ &= \sum_{\mathbf{k} \in \tau_z} \frac{i\pi e^3}{\hbar^2 V} \partial_{k_a} E_{\mathbf{k},12} \Omega_{\tau_z}^v(\mathbf{k}) \delta(\hbar\omega - E_{\mathbf{k},21})\end{aligned}\quad (2)$$

where a, b and c indicate Cartesian indices, a indicates the direction of the current, and b and c are the polarization directions of the optical electric field. At a given frequency ω , the delta function selects the surface in \mathbf{k} space where $E_{\mathbf{k},21} = \hbar\omega$. Note that the CPGE induced valley-dependent photocurrent changes its sign if the Berry curvature changes its sign. If $\eta_{K/K'} = \pm 1$ with no applied out-of-plane electric field, the CPGE tensor $\beta_{bc}^{a,K/K'}$ originates purely from the left/right circularly polarized light contribution. When the out-of-plane electric field is applied, $\eta_{K/K'}$ becomes ∓ 1 and then $\beta_{bc}^{a,K/K'}$ is purely from the right/left circularly polarized light contribution. Consequently, the valley-dependent CPGE tensor $\beta_{bc}^{a,K/K'}$ changes its sign. This suggests that the fully valley-polarized current can be switched between K and K' valleys when a specific handed polarized light is shining. Therefore, it is essential to find a kind of system that can use out-of-plane electric field to adjust the sign of the Berry curvature.

To achieve this, we consider the Dirac Hamiltonian⁴⁶⁻⁴⁹

$$H = \hbar v_f (k_x \hat{\sigma}_x + \hat{\tau}_z k_y \hat{\sigma}_y) + \lambda_{SO} \hat{s}_z \hat{\tau}_z \hat{\sigma}_z + U \hat{\sigma}_z, \quad (3)$$

where v_f is the Fermi velocity. $\hat{\sigma}$ is the Pauli matrix denoting orbital. \hat{s}_z and $\hat{\tau}_z$ represent the spin and valley operator, respectively. λ_{SO} is the intrinsic spin orbital coupling (SOC) strength. U stands for the staggered potential, which can be controlled by the out-of-plane electric field E_{\perp} . By diagonalizing the Hamiltonian in Eq. (3), we find that the energy spectrum is

$$E = \pm \sqrt{(U + \lambda_{SO} s_z \tau_z)^2 + \hbar^2 k^2 v_f^2}. \quad (4)$$

Here, $s_z = \pm 1$ represents the spin up and down components, respectively.

The spin-dependent out-of-plane Berry curvature of the valence bands in different valleys is given by

$$\Omega_{\tau_z}^{s_z}(\mathbf{k}) = -\frac{\hbar^2 v_f^2 \tau_z (U + \lambda_{SO} s_z \tau_z)}{((U + \lambda_{SO} s_z \tau_z)^2 + \hbar^2 k^2 v_f^2)^{3/2}}. \quad (5)$$

From Eq. (5), we can know that the sign of Berry curvature $\text{sgn}(\Omega_K^{\uparrow}, \Omega_K^{\downarrow}, \Omega_{K'}^{\uparrow}, \Omega_{K'}^{\downarrow}) = (-, +, -, +)$ when $|U| < \lambda_{SO}$. The topological charge $C_{\tau_z}^{s_z}$ can be obtained by integrating the Berry curvatures. In this situation, the system resides in the QSHE phase with $(C_K^{\uparrow}, C_K^{\downarrow}, C_{K'}^{\uparrow}, C_{K'}^{\downarrow}) = (-0.5, 0.5, -0.5, 0.5)$ and spin Chern number -1 . When $|U| > \lambda_{SO}$, the sign of Berry curvature becomes

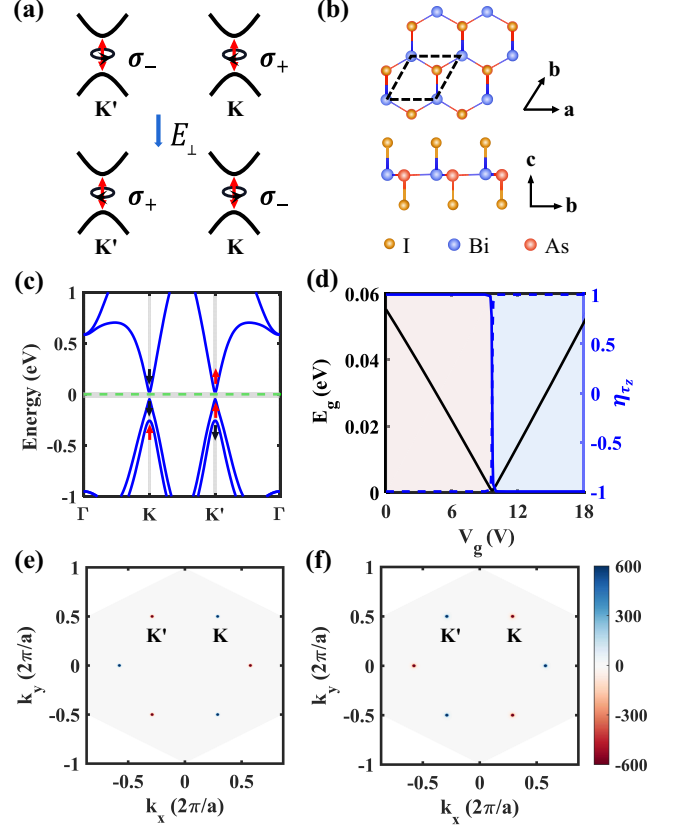


FIG. 1. (a) Schematic of proposed valley-dependent optical selection rules switching at K and K' by applying an out-of-plane electric field E_{\perp} . (b) Crystal structure and (c) band structure of monolayer BiAsI_2 . The horizontal green dashed line denotes the Fermi energy. (d) The band gap E_g and the degree of circular polarization η_{τ_z} at K and K' valleys vs the applied perpendicular gate voltage V_g . The solid and dashed blue lines represent K and K' valleys, respectively. (e, f) The Berry curvatures of the valence band for monolayer BiAsI_2 in the Brillouin zone when $V_g = 0, 18$ V, respectively.

$\text{sgn}(\Omega_K^{\uparrow}, \Omega_K^{\downarrow}, \Omega_{K'}^{\uparrow}, \Omega_{K'}^{\downarrow}) = \text{sgn}(U)(-, -, +, +)$. Correspondingly, the system is in the QVHE phase with $(C_K^{\uparrow}, C_K^{\downarrow}, C_{K'}^{\uparrow}, C_{K'}^{\downarrow}) = \text{sgn}(U)(-0.5, -0.5, 0.5, 0.5)$.

We can reverse the sign of the Berry curvature by tuning U via the external electric field. According to Eqs. (4) and (5), the top of the valence band, when $0 < U < \lambda_{SO}$, is spin down/up in K/K' valleys with sign of Berry curvature $\text{sgn}(\Omega_K^{\downarrow}, \Omega_{K'}^{\uparrow}) = (+, -)$. As U increases beyond λ_{SO} , the sign of Berry curvatures in both valleys reverses, i.e., $\text{sgn}(\Omega_K^{\downarrow}, \Omega_{K'}^{\uparrow}) = (-, +)$. Similarly, when $0 < -U < \lambda_{SO}$, the top of the valence band is spin up/down in K/K' valleys with sign of Berry curvature $\text{sgn}(\Omega_K^{\uparrow}, \Omega_{K'}^{\downarrow}) = (-, +)$. As $-U$ increases beyond λ_{SO} , the sign of Berry curvatures in both valleys also reverses, i.e., $\text{sgn}(\Omega_K^{\uparrow}, \Omega_{K'}^{\downarrow}) = (+, -)$. Moreover, one can directly tune U between the $-U > \lambda_{SO}$ and $U > \lambda_{SO}$ regimes. As a result, the sign of Berry curvature can be switched between $\text{sgn}(\Omega_K^{\uparrow}, \Omega_{K'}^{\downarrow}) = (+, -)$ and $\text{sgn}(\Omega_K^{\downarrow}, \Omega_{K'}^{\uparrow}) = (-, +)$ with spin switching in the specific

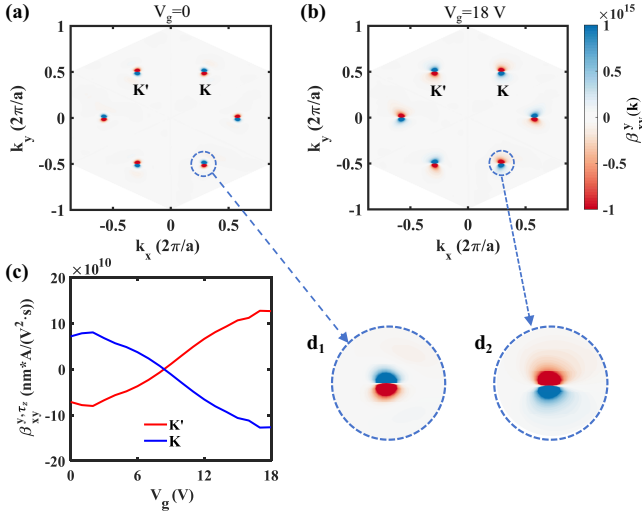


FIG. 2. (a,b) The \mathbf{k} -specified contribution to the CPGE tensor $\beta_{xy}^y(\mathbf{k})$ of monolayer BiAsI₂ in the Brillouin zone when $V_g = 0, 18$ V, respectively. (c) The valley-dependent CPGE tensor β_{xy}^{y,τ_z} vs the gate voltage V_g . Here, the incident photon energy is fixed at $\hbar\omega = 0.06$ eV. (d₁, d₂) Zoom in on the distribution of $\beta_{xy}^y(\mathbf{k})$ near the K valley when $V_g = 0, 18$ V, respectively.

valley.

Fully valley-polarized photocurrent switch—After understanding the proposed underlying mechanism of valley switching, we illustrate the switch of fully valley-polarized photocurrent through an out-of-plane electric field in monolayer BiAsI₂ first. The crystal structure of monolayer BiAsI₂, which has a hexagonal lattice with broken inversion symmetry, is depicted in Fig. 1 (b). Fig. 1 (c) shows the electronic properties of monolayer BiAsI₂ and its low energy physics can be well described by Eq. (3)⁴⁸. Based on the first-principles calculations,⁵⁰ (see also references^{51,52} therein) the monolayer BiAsI₂ is in a QSHE state with a direct bandgap of approximately 58 meV when SOC is considered. The maximum of the valence band and the minimum of the conduction band are located at the K/K' valley with spin down/up components. When an external out-of-plane electric field is applied, the bandgap of monolayer BiAsI₂ gradually decreases and closes as the electric field increases. As the field continues to increase, the bandgap reopens, and monolayer BiAsI₂ undergoes a topological phase transition (TPT) from QSHE to QVHE, as illustrated in Fig. 1 (d) and Supplemental Materials Fig. S1⁵⁰. Figs. 1 (e) and (f) display the Berry curvature distribution for the valence band in the first Brillouin zone before and after the TPT, respectively. It can be observed that the Berry curvature in the K/K' valley changes sign when an external out-of-plane gate voltage is applied. Correspondingly, η_{τ_z} at K/K' switches from ± 1 to ∓ 1 , as shown in Fig. 1 (d).

Next, we calculate the \mathbf{k} -specified CPGE tensor $\beta_{xy}^y(\mathbf{k})$ of monolayer BiAsI₂ as shown in Fig. 2 (a). We find that the CPGE tensor $\beta_{xy}^y(\mathbf{k})$ at K and K' valleys has a “dipole” distribution with opposite signs. From Eq. (2), we learn that $\beta_{xy}^y(\mathbf{k})$ also depends on $\partial E/\partial k_y$, which represents the electron’s velocity in the y -direction. Since there is no mirror sym-

metry in the y -direction, the electron velocity shows opposite signs but different magnitudes in the $k_y < 0$ and $k_y > 0$ regions. As a result, $\beta_{xy}^y(\mathbf{k})$ at $k_y < 0$ and $k_y > 0$ have opposite signs and do not entirely offset each other. When applying an out-of-plane electric field with gate voltage $V_g = 18$ V⁵³, the dipole distribution of the CPGE tensor $\beta_{xy}^{y,\tau_z}(\mathbf{k})$ at K/K' valleys reverses, as Fig. 2 (b) shows. In Fig. 2 (c), we present the valley-dependent CPGE tensor β_{xy}^{y,τ_z} vs the gate voltage. As the gate voltage increases, the CPGE tensor β_{xy}^{y,τ_z} of the K valley switches from positive to negative, while the K' valley’s component changes from negative to positive. This suggests a valley photocurrent switch for certain σ_{\pm} circularly polarized light.

Since the CPGE involves σ_+ and σ_- together, we then calculate the valley-polarized photoresponse at K and K' valleys under certain σ_-/σ_+ circularly polarized light using the non-equilibrium Green’s function combined with density functional theory (NEGF-DFT) formalism^{40,54}. A two-probe transport device is built based on monolayer BiAsI₂ valley materials as shown in Fig. 3 (a). In the numerical simulations, the device can be divided into three regions: the central scattering region where the light is shining, and the left and right leads that extend to the electron reservoirs in infinity as shown in Fig. 3 (e). There are five unit cells with a total of 40 atoms in the central scattering region, about 44.23 Å. During the simulation, along the z direction, vacuum layers of 9.5 Å were added to the top and bottom of the device to avoid the fake interaction between neighboring slabs. Here, back gates are applied throughout the system as shown in Fig. 3 (e) to achieve the gate effect by setting a gate-induced electrostatic boundary condition for the Hartree potential when solving the Poisson equation during the self-consistent calculations.

After obtaining the NEGF-DFT self-consistent device Hamiltonian, the valley-polarized photocurrent flowing in the left electrode, $J_{L,\tau_z}^{(ph)}$, can be expressed using the following formula,^{40,55}

$$\begin{aligned} J_{L,\tau_z}^{(ph)} &= \frac{e}{\hbar} \sum_{\mathbf{k} \in \tau_z} \int T_{eff}(\epsilon, \mathbf{k}) d\epsilon \\ &= \frac{ie}{\hbar} \sum_{\mathbf{k} \in \tau_z} \int \text{Tr}\{\Gamma_L [G_{ph}^< + f_L(\epsilon)(G_{ph}^> - G_{ph}^<)]\} d\epsilon, \end{aligned} \quad (6)$$

where L indicates the left lead; $\Gamma_L = i(\Sigma_L^r - \Sigma_L^a)$ is the linewidth function and $\Sigma_L^r = [\Sigma_L^a]^\dagger$ is the retarded self-energy due to the presence of the left lead; $G_{ph}^{</>} = G_0^r \Sigma_{ph}^{</>} G_0^a$ represents the lesser/greater Green’s function including the electron-photon interaction,⁵⁶ where the $G_0^{r/a}$ is the retarded/advanced Green’s functions without photons and $\Sigma_{ph}^{</>}$ is the self-energy due to the presence of the electron-photon interaction; $f_L(E)$ is the Fermi-Dirac distribution function of the left lead. $T_{eff}(\epsilon, \mathbf{k})$ is the effective transmission coefficient. The polarization of the light can be defined by a complex vector \mathbf{e} . For circularly polarized light, $\mathbf{e} = \frac{1}{\sqrt{2}}(\mathbf{e}_1 \pm i\mathbf{e}_2)$.⁵⁷ In our numerical calculations, the vectors \mathbf{e}_1 and \mathbf{e}_2 are set along the y and x directions and the light is incident along the $-z$ direction as shown in Fig. 3 (e).

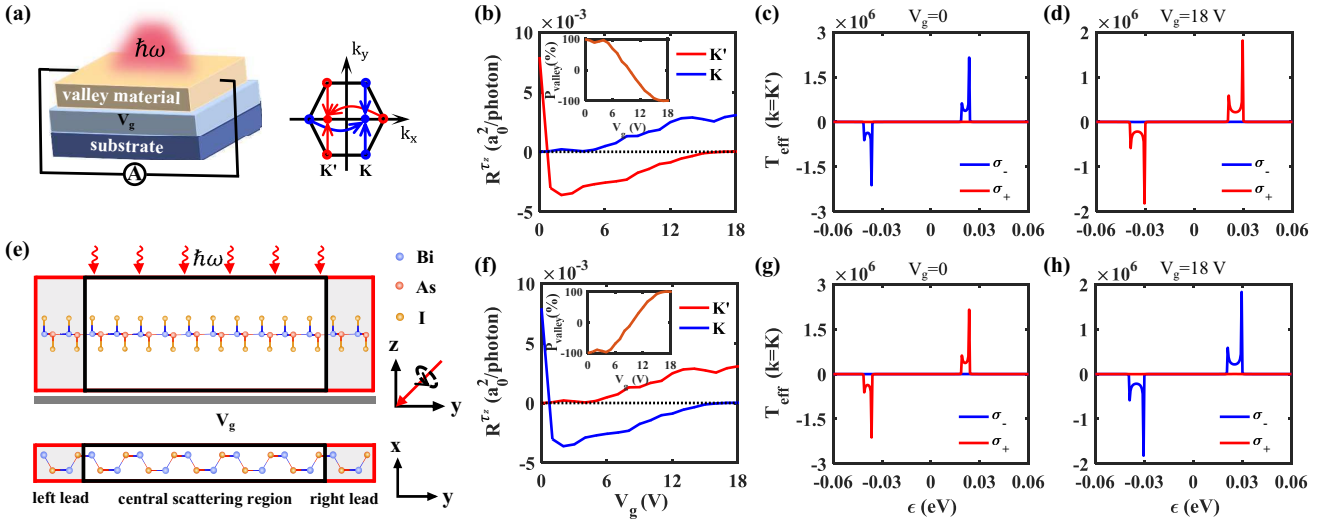


FIG. 3. (a) The proposed opto-valleytronic device based on two-dimensional valley materials and the corresponding folded Brillouin zone. (e) Schematic plot of the two-probe device constructed by monolayer BiAsI₂. The blue, red and yellow spheres represent Bi, As, and I atoms, respectively. (b, f) The valley-polarized photoresponse $R^{\tau z}$ vs the gate voltage V_g under the vertically incident (b) σ_- , (f) σ_+ circularly polarized light, respectively. Insets show the corresponding valley polarization vs V_g . (c, g) The effective transmission T_{eff} vs ϵ at K' and K points when $V_g = 0$ V. (d, h) The effective transmission T_{eff} vs ϵ at K' and K points when $V_g = 18$ V. Here, the incident photon energy is fixed at $\hbar\omega = 0.06$ eV.

For simplicity, we introduce a normalized valley related photoresponse^{55,56,58},

$$R^{\tau z} = \frac{J_{L,\tau z}^{(ph)}}{eI_\omega}, \quad (7)$$

where the unit of $R^{\tau z}$ is a_0^2/photon and a_0 represents the Bohr radius; I_ω is the photon flux defined as the number of photons per unit time per unit area.

In order to characterize the polarization of the generated valley-polarized photocurrent, the valley polarization (VP) is defined as

$$P_{valley}(\%) = \frac{|R^{K'}| - |R^K|}{|R^{K'}| + |R^K|} \times 100. \quad (8)$$

The valley-polarized photoresponse of a monolayer BiAsI₂ dependence on gate voltage is shown in Figs. 3 (b, f). We note that without an external out-of-plane electric field, the photoresponse at the K' valley can only be stimulated by the σ_- circularly polarized light, creating a valley polarization of 100%. Yet, when a vertical voltage V_g is introduced, the photoresponse at the K' valley decreases, while the photoresponse at the K valley rises. At a gate voltage of 18V, the photoresponse at the K' valley is nearly zero, and the corresponding valley polarization reaches -100% . In contrast, with σ_+ circularly polarized light, the photoresponse at the K' valley grows with the gate voltage, while the photoresponse at the K valley shrinks. Thus, the valley polarization changes from -100 to 100% when the gate voltage of 18V is applied. Figs. 3 (c, g) displays the effective transmission coefficient T_{eff} at the K' and K valleys without gate voltage. It is observed that only the electrons at the K' valley can transport under the

σ_- circularly polarized light, whereas the electrons at the K valley transport under the σ_+ circularly polarized light. However, when the gate voltage $V_g = 18$ V is used, the electrons at the K' valley can transport under the σ_+ circularly polarized light, while the electrons at the K valley operate under the σ_- circularly polarized light, as shown in Figs. 3 (d, h). These directly present a fully valley-polarized photocurrent switch, achieved by applying the out-of-plane electric field to the monolayer BiAsI₂.

Recently, the TPT induced by the out-of-plane electric field in germanene has been successfully confirmed in experiments.^{49,59-61} Consequently, it is promising to realize the fully valley-polarized photocurrent switch based on germanene. Germanene has inversion symmetry, which means the Berry curvature equals zero. When the out-of-plane electric field is applied, this symmetry is broken, leading to a non-zero Berry curvature. The direction of the electric field can control the sign of the Berry curvature. Without an external electric field, germanene is a direct bandgap semiconductor with a bandgap of 20 meV. When a negative gate voltage $V_g = -8$ V is applied, the maximum valence band at the K valley is spin up, while the K' valley is spin down. Reversing the gate voltage V_g to 8V also reverses the spin of the maximum valence band at the K/K' valley, with a TPT transition between QVHE as discussed in the Dirac model analysis, as shown in Figs. 4 (a, b). When the gate voltage changes from -8 to 8V, the band gap closes twice, which is accompanied by a reversal of the circular polarization degree's sign, as illustrated in Fig. 4 (c) and Supplemental Materials Fig. S3⁵⁰. This results in the flipping of the CPGE tensor's sign, which offers the potential to switch the valley photocurrent. The CPGE tensor $\beta_{xy}^y(\mathbf{k})$ at $V_g = \mp 8$ V at K/K' valleys displays an opposite dipole distribution, as shown in Figs. 4 (e)

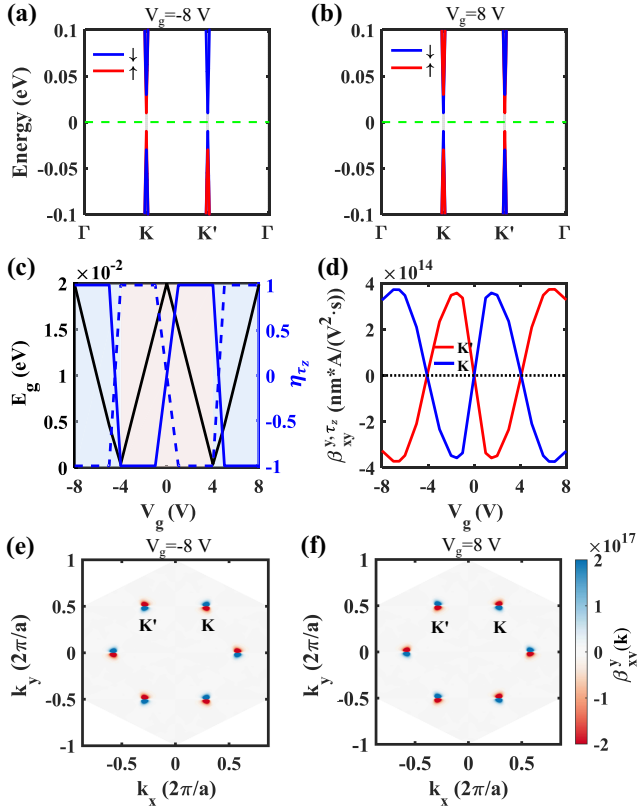


FIG. 4. (a, b) The band structure of germanene when $V_g = \mp 8V$, respectively. The horizontal green dashed line represents the Fermi energy. (c) The band gap E_g and the degree of circular polarization η_{τ_z} at K and K' valleys vs the gate voltage V_g . The solid and dashed blue lines represent K and K' valleys, respectively. (d) The valley-dependent CPGE tensor β_{xy}^{y,τ_z} vs the gate voltage V_g . Here, the incident photon energy is fixed at $\hbar\omega = 0.025$ eV. (e, f) The \mathbf{k} -specified contribution to the CPGE tensor $\beta_{xy}^y(\mathbf{k})$ when $V_g = \mp 8V$, respectively.

and (f). The corresponding dipole distributions at K/K' valleys also reverse through the tuning gate voltage.

Finally, the valley-polarized photoresponse of germanene dependence on gate voltage is shown in Figs. 5 (a, b). When the gate voltage is zero, the Berry curvatures in the Brillouin zone are zero due to the presence of inversion and time reversal symmetries, which in turn results in a zero photoresponse. However, when an out-of-plane electric field is applied, the broken inversion symmetry leads to a non-zero Berry curvature and subsequently, a non-zero photoresponse. When a gate voltage of $-8V$ is applied, the photoresponse at K' valley can only be stimulated by the σ_- circularly polarized light, creating a valley polarization of 100%. Yet, when a vertical voltage $V_g = 8V$ is introduced, the photoresponse at the K' valley is nearly zero, and the corresponding valley polarization reaches -100% . In contrast, with σ_+ circularly polarized light, the photoresponse at the K/K' valley shows the opposite change. Thus, the valley polarization changes from -100 to 100% when the gate voltage of $\mp 8V$ is applied. When calculating the effective transmission coefficients at K/K' valleys with

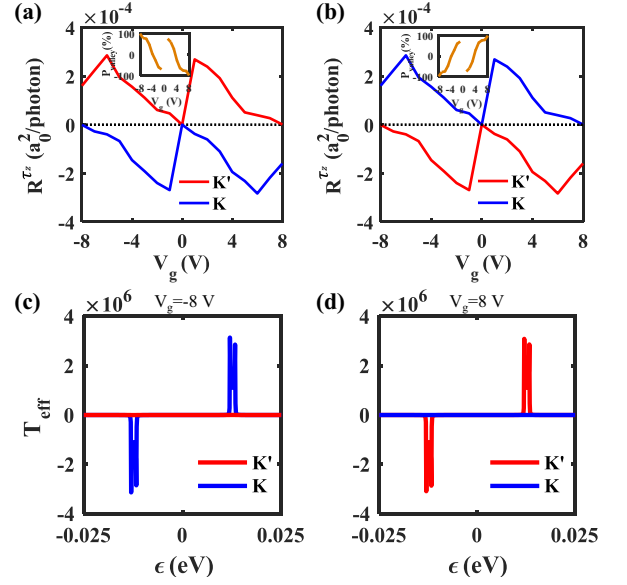


FIG. 5. The valley-polarized photoresponse R^{τ_z} vs the gate voltage V_g under the vertically incident (a) σ_- , (b) σ_+ circularly polarized light, respectively. Inserts show the corresponding valley polarization vs V_g . (c, d) The effective transmission T_{eff} vs ϵ at K and K' points when $V_g = \mp 8V$ of the vertically incident σ_+ circularly polarized light. Here, the incident photon energy is fixed at $\hbar\omega = 0.025$ eV.

σ_+ circular polarized light, we find that when $V_g = -8V$, only the electrons at the K valley can transport, while transported electrons at the K' valley are forbidden. When $V_g = 8V$, the valley-dependent optical selection rule changes. As a result, only the electrons at the K' valley can transport, while the transport of electrons at the K valley are forbidden. This confirms that by controlling the direction of the electric field, we can realize a valley switch based on germanene. It is important to note that the valley-polarized photocurrent produced in germanene is symmetrical with the gate voltage. This is because of the presence of inversion symmetry when there is no gate voltage. In contrast, the valley polarized photocurrent in monolayer BiAsI_2 is expected to be asymmetrical due to its lower symmetry.

Conclusions—To summarize, we propose a scheme of a valley switch by electric field. This method allows for effective control of valley polarization, resulting in valley photocurrents with opposite valley indices. Using first-principles calculation, we successfully realize the switching of valley-polarized photocurrent using the electric field in monolayer BiAsI_2 and germanene. The corresponding valley polarization can be switched between 100 and -100% by applying the out-of-plane electric field. This opens up new possibilities for the development of future valley-based electronic storage devices.

ACKNOWLEDGMENTS

We gratefully acknowledge the support from the National Key Research and Development Program of China (Grant

No. 2022YFA1404003), the National Natural Science Foundation of China (Grants No. 12074230, No. 12034014, and No. 12174231), the Fund for Shanxi “1331 Project”, Fundamental Research Program of Shanxi Province (Grant No. 202103021222001), Research Project Supported by Shanxi Scholarship Council of China, and the Graduate Education Innovation Project of Shanxi Province (Grant No. 2023KY013).

This research was partially conducted using the High Performance Computer of Shanxi University.

*) chenjun@sxu.edu.cn

†) zhanglei@sxu.edu.cn

‡) jianwang@hku.hk

- ¹ Ting Cao, Gang Wang, Wenpeng Han, Huiqi Ye, Chuanrui Zhu, Junren Shi, Qian Niu, Pingheng Tan, Enge Wang, Baoli Liu, and Ji Feng, “Valley-selective circular dichroism of monolayer molybdenum disulphide,” *Nature communications* **3**, 887 (2012).
- ² Jan Isberg, Markus Gabrysch, Johan Hammersberg, Saman Majidi, Kiran Kumar Kovi, and Daniel J Twitchen, “Generation, transport and detection of valley-polarized electrons in diamond,” *Nature materials* **12**, 760–764 (2013).
- ³ Atsufumi Hirohata and Koki Takanashi, “Future perspectives for spintronic devices,” *Journal of Physics D: Applied Physics* **47**, 193001 (2014).
- ⁴ Bernhard Urbaszek and Xavier Marie, “Divide and polarize,” *Nature Physics* **11**, 94–95 (2015).
- ⁵ Hongyi Yu and Wang Yao, “Magnetization without polarization,” *Nature Materials* **16**, 876–877 (2017).
- ⁶ John R Schaibley, Hongyi Yu, Genevieve Clark, Pasqual Rivera, Jason S Ross, Kyle L Seyler, Wang Yao, and Xiaodong Xu, “Valleytronics in 2d materials,” *Nature Reviews Materials* **1**, 1–15 (2016).
- ⁷ Andrea Candini, Svetlana Klyatskaya, Mario Ruben, Wolfgang Wernsdorfer, and Marco Affronte, “Graphene spintronic devices with molecular nanomagnets,” *Nano Letters* **11**, 2634–2639 (2011).
- ⁸ YoshiChika Otani, Masashi Shiraishi, Akira Oiwa, Eiji Saitoh, and Shuichi Murakami, “Spin conversion on the nanoscale,” *Nature Physics* **13**, 829–832 (2017).
- ⁹ Søren Schou Gregersen, Stephen R Power, and Antti-Pekka Jauho, “Nanostructured graphene for spintronics,” *Physical Review B* **95**, 121406 (2017).
- ¹⁰ Ethan C Ahn, “2d materials for spintronic devices,” *npj 2D Materials and Applications* **4**, 1–14 (2020).
- ¹¹ Di Xiao, Wang Yao, and Qian Niu, “Valley-contrasting physics in graphene: magnetic moment and topological transport,” *Physical Review Letters* **99**, 236809 (2007).
- ¹² A. Rycerz, J. Tworzydło, and C. W. J. Beenakker, “Valley filter and valley valve in graphene,” *Nature Physics* **3**, 172–175 (2007).
- ¹³ Mengqiao Sui, Guorui Chen, Liguo Ma, Wen-Yu Shan, Dai Tian, Kenji Watanabe, Takashi Taniguchi, Xiaofeng Jin, Wang Yao, Di Xiao, and Yuanbo Zhang, “Gate-tunable topological valley transport in bilayer graphene,” *Nature Physics* **11**, 1027–1031 (2015).
- ¹⁴ Di Xiao, Gui-Bin Liu, Wanxiang Feng, Xiaodong Xu, and Wang Yao, “Coupled spin and valley physics in monolayers of mos2 and other group-vi dichalcogenides,” *Physical Review Letters* **108**, 196802 (2012).
- ¹⁵ Kin Fai Mak, Kathryn L McGill, Jiwoong Park, and Paul L McEuen, “The valley hall effect in mos2 transistors,” *Science* **344**, 1489–1492 (2014).
- ¹⁶ Jieun Lee, Kin Fai Mak, and Jie Shan, “Electrical control of the valley hall effect in bilayer mos2 transistors,” *Nature nanotechnology* **11**, 421–425 (2016).
- ¹⁷ Bairen Zhu, Hualing Zeng, Junfeng Dai, Zhirui Gong, and Xiaodong Cui, “Anomalously robust valley polarization and valley coherence in bilayer ws2,” *Proceedings of the National Academy of Sciences* **111**, 11606–11611 (2014).
- ¹⁸ Fuming Xu, Zhizhou Yu, Yafei Ren, Bin Wang, Yadong Wei, and Zhenhua Qiao, “Transmission spectra and valley processing of graphene and carbon nanotube superlattices with inter-valley coupling,” *New Journal of Physics* **18**, 113011 (2016).
- ¹⁹ Zhi-Ming Yu, Shan Guan, Xian-Lei Sheng, Weibo Gao, and Shengyuan A. Yang, “Valley-layer coupling: a new design principle for valleytronics,” *Physical Review Letters* **124**, 037701 (2020).
- ²⁰ Kai-Tong Wang, Hui Wang, Fuming Xu, Yunjin Yu, and Yadong Wei, “Realization of valley-spin polarized current via parametric pump in monolayer mos2,” *New Journal of Physics* **25**, 013019 (2023).
- ²¹ Yilei Li, Jonathan Ludwig, Tony Low, Alexey Chernikov, Xu Cui, Ghidewon Arefe, Young Duck Kim, Arend M. Van Der Zande, Albert Rigosi, Heather M. Hill, Suk Hyun Kim, James Hone, Zhiqiang Li, Dmitry Smirnov, and Tony F. Heinz, “Valley splitting and polarization by the zeeman effect in monolayer mose2,” *Physical Review Letters* **113**, 266804 (2014).
- ²² Chuan Zhao, Tenzin Norden, Peiyao Zhang, Puqin Zhao, Yingchun Cheng, Fan Sun, James P. Parry, Payam Taheri, Jieqiong Wang, Yihang Yang, Thomas Scrace, Kaifei Kang, Sen Yang, Guo-xing Miao, Renat Sabirianov, George Kioseoglou, Wei Huang, Athos Petrou, and Hao Zeng, “Enhanced valley splitting in monolayer wse2 due to magnetic exchange field,” *Nature nanotechnology* **12**, 757–762 (2017).
- ²³ Hualing Zeng, Junfeng Dai, Wang Yao, Di Xiao, and Xiaodong Cui, “Valley polarization in mos2 monolayers by optical pumping,” *Nature nanotechnology* **7**, 490–493 (2012).
- ²⁴ Kin Fai Mak, Keliang He, Jie Shan, and Tony F. Heinz, “Control of valley polarization in monolayer mos2 by optical helicity,” *Nature nanotechnology* **7**, 494–498 (2012).
- ²⁵ Motohiko Ezawa, “Valley-polarized metals and quantum anomalous hall effect in silicene,” *Physical Review Letters* **109**, 055502 (2012).
- ²⁶ Yuya Shimazaki, Michihisa Yamamoto, Ivan V. Borzenets, Kenji Watanabe, Takashi Taniguchi, and Seigo Tarucha, “Generation and detection of pure valley current by electrically induced berry curvature in bilayer graphene,” *Nature Physics* **11**, 1032–1036 (2015).
- ²⁷ Ao Zhang, Kaike Yang, Yun Zhang, Anlian Pan, and Mingxing Chen, “Electrically switchable valley polarization, spin/valley filter, and valve effects in transition-metal dichalcogenide monolayers interfaced with two-dimensional ferromagnetic semiconductors,” *Physical Review B* **104**, L201403 (2021).
- ²⁸ Yu Ye, Jun Xiao, Hailong Wang, Ziliang Ye, Hanyu Zhu, Mervin Zhao, Yuan Wang, Jianhua Zhao, Xiaobo Yin, and Xiang Zhang, “Electrical generation and control of the valley carriers in a monolayer transition metal dichalcogenide,” *Nature nanotechnology* **11**, 598–602 (2016).

- ²⁹ Yang Li, Yizhou Liu, Chong Wang, Jianfeng Wang, Yong Xu, and Wenhui Duan, “Electrically tunable valleytronics in quantum anomalous hall insulating transition metal trihalides,” *Physical Review B* **98**, 201407 (2018).
- ³⁰ Li Liang, Ying Yang, Xiaohui Wang, and Xiao Li, “Tunable valley and spin splittings in vsi2n4 bilayers,” *Nano Letters* **23**, 858–862 (2023).
- ³¹ Xiaodong Zhou, Run-Wu Zhang, Zeying Zhang, Wanxiang Feng, Yuriy Mokrousov, and Yugui Yao, “Sign-reversible valley-dependent berry phase effects in 2d valley-half-semiconductors,” *npj Computational Materials* **7**, 160 (2021).
- ³² Lizhong Li, Shengwei Jiang, Zefang Wang, Kenji Watanabe, Takashi Taniguchi, Jie Shan, and Kin Fai Mak, “Electrical switching of valley polarization in monolayer semiconductors,” *Physical Review Materials* **4**, 104005 (2020).
- ³³ Imran Khan, Brahim Marfoua, and Jisang Hong, “Electric field induced giant valley polarization in two dimensional ferromagnetic wse2/crsnse3 heterostructure,” *npj 2D Materials and Applications* **5**, 10 (2021).
- ³⁴ Zhiming Yu, Hui Pan, and Yugui Yao, “Electric field controlled spin-and valley-polarized edge states in silicene with extrinsic rashba effect,” *Physical Review B* **92**, 155419 (2015).
- ³⁵ Huiping Li and Wenguang Zhu, “Spin-driven ferroelectricity in two-dimensional magnetic heterostructures,” *Nano Letters* **23**, 10651–10656 (2023).
- ³⁶ Hongtao Yuan, Xinqiang Wang, Biao Lian, Haijun Zhang, Xianfa Fang, Bo Shen, Gang Xu, Yong Xu, Shou-Cheng Zhang, Harold Y. Hwang, and Yi Cui, “Generation and electric control of spin-valley-coupled circular photogalvanic current in wse2,” *Nature nanotechnology* **9**, 851–857 (2014).
- ³⁷ Lei Liu, Erik J. Lenferink, Guohua Wei, Teodor K. Stanev, Nathaniel Speiser, and Nathaniel P. Stern, “Electrical control of circular photogalvanic spin-valley photocurrent in a monolayer semiconductor,” *ACS applied materials & interfaces* **11**, 3334–3341 (2019).
- ³⁸ Yunqiu Kelly Luo, Jinsong Xu, Tiancong Zhu, Guanzhong Wu, Elizabeth J. McCormick, Wenbo Zhan, Mahesh R. Neupane, and Roland K. Kawakami, “Opto-valleytronic spin injection in monolayer mos2/few-layer graphene hybrid spin valves,” *Nano Letters* **17**, 3877–3883 (2017).
- ³⁹ Sangeeta Sharma, Deepika Gill, and Samuel Shallcross, “Giant and controllable valley currents in graphene by double pumped thz light,” *Nano Letters* **23**, 10305–10310 (2023).
- ⁴⁰ Lei Zhang, Kui Gong, Jingzhe Chen, Lei Liu, Yu Zhu, Di Xiao, and Hong Guo, “Generation and transport of valley-polarized current in transition-metal dichalcogenides,” *Physical Review B* **90**, 195428 (2014).
- ⁴¹ J. E. Sipe and A. I. Shkrebtii, “Second-order optical response in semiconductors,” *Physical Review B* **61**, 5337 (2000).
- ⁴² Su-Yang Xu, Qiong Ma, Huitao Shen, Valla Fatemi, Sanfeng Wu, Tay-Rong Chang, Guoqing Chang, Andrés M. Mier Valdivia, Ching-Kit Chan, Quinn D. Gibson, Jiadong Zhou, Zheng Liu, Kenji Watanabe, Takashi Taniguchi, Hsin Lin, Robert J. Cava, Liang Fu, Nuh Gedik, and Jarillo-Herrero Pablo, “Electrically switchable berry curvature dipole in the monolayer topological insulator wte2,” *Nature Physics* **14**, 900–906 (2018).
- ⁴³ Wang Yao, Di Xiao, and Qian Niu, “Valley-dependent optoelectronics from inversion symmetry breaking,” *Physical Review B* **77**, 235406 (2008).
- ⁴⁴ Fernando De Juan, Adolfo G. Grushin, Takahiro Morimoto, and Joel E. Moore, “Quantized circular photogalvanic effect in weyl semimetals,” *Nature communications* **8**, 15995 (2017).
- ⁴⁵ Haowei Xu, Hua Wang, Jian Zhou, and Ju Li, “Pure spin photocurrent in non-centrosymmetric crystals: bulk spin photovoltaic effect,” *Nature communications* **12**, 4330 (2021).
- ⁴⁶ Cheng-Cheng Liu, Wanxiang Feng, and Yugui Yao, “Quantum spin hall effect in silicene and two-dimensional germanium,” *Physical Review Letters* **107**, 076802 (2011).
- ⁴⁷ Cheng-Cheng Liu, Hua Jiang, and Yugui Yao, “Low-energy effective hamiltonian involving spin-orbit coupling in silicene and two-dimensional germanium and tin,” *Physical Review B* **84**, 195430 (2011).
- ⁴⁸ Tong Zhou, Shuguang Cheng, Michael Schleenvoigt, Peter Schüffelgen, Hua Jiang, Zhongqin Yang, and Igor Žutić, “Quantum spin-valley hall kink states: From concept to materials design,” *Physical Review Letters* **127**, 116402 (2021).
- ⁴⁹ Pantelis Bampoulis, Carolien Castenmiller, Dennis J. Klaassen, Jelle van Mil, Yichen Liu, Cheng-Cheng Liu, Yugui Yao, Motohiko Ezawa, Alexander N. Rudenko, and Harold J. W. Zandvliet, “Quantum spin hall states and topological phase transition in germanene,” *Physical Review Letters* **130**, 196401 (2023).
- ⁵⁰ See Supplemental Material at <http://link.aps.org/supplemental/XXX> for detailed information on the first principle calculations, which includes Refs. [40–42, 44, 48, 51, 52, 54, 59, 61–64].
- ⁵¹ Leonard Kleinman and D. M. Bylander, “Efficacious form for model pseudopotentials,” *Physical Review Letters* **48**, 1425–1428 (1982).
- ⁵² Georg Kresse and Jürgen Hafner, “Ab initio molecular dynamics for liquid metals,” *Physical Review B* **47**, 558–561 (1993).
- ⁵³ The strength of the gate voltage may be realized in the experiments.^{65–68}
- ⁵⁴ Jeremy Taylor, Hong Guo, and Jian Wang, “Ab initio modeling of quantum transport properties of molecular electronic devices,” *Physical Review B* **63**, 245407 (2001).
- ⁵⁵ Jingzhe Chen, Yibin Hu, and Hong Guo, “First-principles analysis of photocurrent in graphene *pn* junctions,” *Physical Review B* **85**, 155441 (2012).
- ⁵⁶ Lindor E. Henrickson, “Nonequilibrium photocurrent modeling in resonant tunneling photodetectors,” *Journal of applied physics* **91**, 6273–6281 (2002).
- ⁵⁷ Yiqun Xie, Lei Zhang, Yu Zhu, Lei Liu, and Hong Guo, “Photogalvanic effect in monolayer black phosphorus,” *Nanotechnology* **26**, 455202 (2015).
- ⁵⁸ Jun Chen, Liwen Zhang, Lei Zhang, Xiaohong Zheng, Liantuan Xiao, Suotang Jia, and Jian Wang, “Photogalvanic effect induced fully spin polarized current and pure spin current in zigzag sic nanoribbons,” *Physical Chemistry Chemical Physics* **20**, 26744–26751 (2018).
- ⁵⁹ Arka Bandyopadhyay, Nesta Benno Joseph, and Awadhesh Narayan, “Electrically switchable giant berry curvature dipole in silicene, germanene and stanene,” *2D Materials* **9**, 035013 (2022).
- ⁶⁰ Linfei Li, Shuang-zan Lu, Jinbo Pan, Zhihui Qin, Yu-qi Wang, Yeliang Wang, Geng-yu Cao, Shixuan Du, and Hong-Jun Gao, “Buckled germanene formation on pt (111),” *Advanced Materials* **26**, 4820–4824 (2014).
- ⁶¹ Jialiang Deng, Bingyu Xia, Xiaochuan Ma, Haoqi Chen, Huan Shan, Xiaofang Zhai, Bin Li, Aidi Zhao, Yong Xu, Wenhui Duan, Shou-Cheng Zhang, Bing Wang, and J. G. Hou, “Epitaxial growth of ultraflat stanene with topological band inversion,” *Nature materials* **17**, 1081–1086 (2018).
- ⁶² G. Kresse and J. Furthmüller, “Efficient iterative schemes for ab initio total-energy calculations using a plane-wave basis set,” *Physical Review B* **54**, 11169–11186 (1996).
- ⁶³ For details of the NanoDcal quantum transport package, see <http://www.hzwtech.com>.
- ⁶⁴ John P. Perdew, Kieron Burke, and Matthias Ernzerhof, “Generalized gradient approximation made simple,” *Physical Review*

- [Letters](#) **77**, 3865 (1996).
- ⁶⁵ Yuanbo Zhang, Tsung-Ta Tang, Caglar Girit, Zhao Hao, Michael C Martin, Alex Zettl, Michael F Crommie, Y Ron Shen, and Feng Wang, “Direct observation of a widely tunable bandgap in bilayer graphene,” [Nature](#) **459**, 820–823 (2009).
- ⁶⁶ Hanwen Wang, Mao-Lin Chen, Mengjian Zhu, Yaning Wang, Baojuan Dong, Xingdan Sun, Xiaorong Zhang, Shimin Cao, Xiaoxi Li, Jianqi Huang, *et al.*, “Gate tunable giant anisotropic resistance in ultra-thin gate,” [Nature communications](#) **10**, 2302 (2019).
- ⁶⁷ Benjamin I Weintrub, Yu-Ling Hsieh, Sviatoslav Kovalchuk, Jan N Kirchhof, Kyrylo Greben, and Kirill I Bolotin, “Generating intense electric fields in 2d materials by dual ionic gating,” [Nature Communications](#) **13**, 6601 (2022).
- ⁶⁸ Cheng Tan, Ji-Hai Liao, Guolin Zheng, Meri Algarni, Jia-Yi Lin, Xiang Ma, Edwin LH Mayes, Matthew R Field, Sultan Albarakati, Majid Panahandeh-Fard, *et al.*, “Room-temperature magnetic phase transition in an electrically tuned van der waals ferromagnet,” [Physical Review Letters](#) **131**, 166703 (2023).